Structure and vibrational spectra of methanol clusters from a new potential model

Udo Buck and Jörg-Gerald Siebers
Max-Planck-Institut für Srömungsforschung, Bunsenstrasse 10, D-37073 Göttingen, Germany

Richard J. Wheatley[a)]
Department of Chemistry, University of Durham, Durham DH1 3LE, England

(Received 23 July 1997; accepted 23 September 1997)

The structures and vibrational spectra of small methanol clusters from dimer to decamer have been calculated using a newly developed intermolecular potential which is essentially based on monomer wave functions. Special care has been taken for the description of the electrostatic interaction using a distributed multipole representation and including a penetration term. In addition, the potential model consists of repulsion, dispersion, and induction terms. Based on this potential model cluster structures have been calculated. The lowest energy dimer configuration is linear, while from trimer to decamer for the most stable structures ring configurations were found. Tetramer, hexamer, and octamer have S_4-, S_6-, and S_8-symmetry, respectively. Vibrational spectra of the CO stretch and the OH stretch mode have been determined in the harmonic and in the anharmonic approximation using perturbation theory and variational calculations. Up to the tetramer the experimental spectra of the CO stretch mode are well reproduced, for larger clusters an increasing blueshift with respect to the experimental evidence is found. The experimental data for the OH stretch mode of the dimer are fairly well reproduced in all approximations, however, the spectrum of the trimer can only be reproduced using the variational calculation which includes Darling–Dennison resonance terms. [S0021-9606(98)00201-3]

I. INTRODUCTION

Small methanol clusters are bound by linear hydrogen bonds which determine their typical structure. Considerable efforts have been spent to get information on the nature of these clusters using mainly spectroscopic methods. The vibrational spectrum of a single cluster isomer can be viewed as a fingerprint which can be identified using realistic interaction potentials and precise methods to calculate the energy eigenvalues of the cluster states that are accessible.

In principle experimental high resolution techniques using absorption[1,2] or opto-thermal detection[3,4] are the methods of choice. These methods are restricted to very small systems, however. As the production of clusters usually leads to a cluster size distribution, size selection is a difficult task to solve. Mass spectrometric methods are not applicable as the ionization process leads to fragmentation which destroys the correlation between the measured ionic cluster and its neutral precursor. Buck and Meyer[5] used the momentum transfer in a scattering experiment to select a neutral cluster of defined size. In combination with subsequent infrared photodissociation spectroscopy information on the structure of a single cluster size is available.[6]

To evaluate the experimental data a comparison with calculated infrared spectra is necessary. Prerequisite is an accurate interaction potential for the determination of cluster structures and of energy eigenvalues. Since the determination of *ab initio* potentials for clusters which include correlation effects and account for anharmonicity is still very expensive, we decided to use separated intra- and intermolecular potentials. This facilitates a large scale search for cluster structures as it reduces the degrees of freedom taken into account drastically. Furthermore a realistic approach for the calculation of the energy eigenvalues is required. Recently we have described an approach for the evaluation of frequency shifts of molecular clusters in various approximations.[7] The basic idea is to construct a (total) cluster potential using separated intra- and intermolecular potential models. Then the normal mode analysis based on the harmonic oscillator is applied. Anharmonicity effects are accounted for using perturbational or variational calculations. We call this procedure the *cluster approach* in contrast to other methods where the intermolecular interaction and the intramolecular anharmonicity are treated as a quantum mechanical perturbation and which thus start from the harmonic frequencies of the bare molecule.[8,9]

Measurements and calculations have been conducted for various molecular clusters including SF_6,[10–12] hydrazine,[13,14] and last but not least methanol clusters. For the latter one experimental data are available for the CO stretch mode[15] from dimer to hexamer and for the OH stretch mode for the dimer[16,17] and the trimer.[18] It is noted that the new experimental results up to the nonamer will be presented in a forthcoming paper.[19]

All calculations for methanol clusters based on separated intra- and intermolecular potentials[7–9] were carried out using the *Optimized Potential for Liquid Simulation* (OPLS) by Jorgensen[20] for the intermolecular part. While a qualitative agreement between measured and calculated data was found

[a)]Present address: Department of Chemistry, University of Nottingham, Nottingham NG7 2RD, England.

 0021-9606/98/108(1)/20/13/$15.00

for the CO stretch mode from dimer to hexamer, the OH stretch mode could not be reproduced. For the dimer a deviation from the experimental value of the donor OH stretch mode of about 100 cm^{-1} is found. For the trimer one infrared active mode is calculated while experimentally three distinct lines are measured. This can be explained by the fact that the energetically most stable structure of the trimer using the OPLS potential has C_{3h}-symmetry in contradiction to *ab initio* calculations in the self-consistent field (SCF) approximation[21,22] which yield a distorted ring configuration with three infrared active modes. For the tetramer again the OPLS structure is a planar ring with C_{4h}-symmetry, while SCF calculations yield a ring configuration with S_4-symmetry. The OPLS binding energy of the clusters is too large, because of a static dipole moment which was chosen to exceed the experimental value by 25% to account for non-additive effects in the liquid phase. This can partly explain the large deviation of the donor OH stretch mode of the dimer from the experimental value. Obviously there is a need for an intermolecular potential that is valid in the microscopic range and that takes special care of the electrostatic interaction because of the hydrogen bonding in methanol clusters.

In this paper we investigate the structural properties of small methanol clusters for $M=2-10$ using a new intermolecular potential which was developed mainly from properties of SCF monomer wave functions. For the electrostatic part of the potential, a distributed multipole expansion and a penetration correction are used. In addition, the potential consists of repulsion, dispersion, and non-additive induction terms. The *cluster approach* was chosen to calculate the spectral line shifts using the new intermolecular potential and a simplified intramolecular force field by Schlegel *et al.*[7,23]

The outline of the paper is as follows: In Sec. II we give a description of the interaction potentials and results for the second virial coefficient. In Sec. III we report structural properties of the clusters and in Sec. IV the *cluster approach* is briefly described. In Sec. V frequency shifts of the CO stretch and the OH stretch mode are given and in Sec. VI we conclude with a discussion of our results.

II. INTERACTION POTENTIALS

A. Systematic intermolecular potential model

In order to describe the different hydrogen-bonded environments of methanol molecules in clusters of differing size, it is most important to have a reasonable representation of the electrostatic interaction between the charge densities of the molecules. This is given exactly by the classical expression

$$E_C^{(1)}=\int\int \rho_A(\mathbf{r}_1)\rho_B(\mathbf{r}_2)(4\pi\epsilon_0 r_{12})^{-1}d\mathbf{r}_1 d\mathbf{r}_2, \qquad (1)$$

where $E_C^{(1)}$ denotes first-order Coulomb energy, and ρ_A and ρ_B are the total (electronic plus nuclear) charge densities of two molecules A and B. For a cluster containing more than two molecules, similar contributions from all pairs of molecules are added to give the total first-order Coulomb energy. Although this method is exact, it is not feasible to evaluate the integrals every time the energy is required. A more practical functional form can be obtained either by evaluating equation (1) directly for a set of intermolecular geometries, and fitting the results to a convenient function, or by making approximations to simplify equation (1), or both. Here, the multipole approximation is used to estimate $E_C^{(1)}$, and the difference between the estimated and exact values is fitted to a simple, short-ranged function.

TABLE I. Distributed multipoles of the methanol molecule, in atomic units (charge/e, dipole/$e\ a_0$, and quadrupole/$e\ a_0^2$). Note that all these values should be multiplied by 1.063 in the intermolecular potential, for calculating the electrostatic, penetration, and induction energies. Very small quadrupoles (less than 0.1 atomic units) are neglected.

Atom	C	O	H (O)
Q_{00} (charge)	0.359480	−0.707559	0.348079
Q_{10} (z dipole)	0.406927	−0.107400	0.032539
Q_{11c} (x dipole)	−0.112357	0.052494	0.033117
Q_{20}	0.315482	0.326724	
Q_{21c}		0.147507	
Q_{22c}		0.331979	0.117546

An approximation to the first-order Coulomb energy, which is reasonable for moderately large intermolecular separations, is to use distributed multipoles[24] to represent the charge densities. In this work, point charges, dipoles, and quadrupoles are used, located at the C, O, and H (O) nuclei; the charge density of the H (C) atoms is incorporated into the carbon atom. It is helpful to consider atom-centered coordinates for each of these nuclei, which are parallel to each other, but with an appropriate shift of origin. The atom-centered point multipoles are calculated from a SCF monomer wave function. The C–O distance is 1.430 Å, O–H is 0.945 Å, and C–H is 1.094 Å, with a COH bond angle of 108.5°, and tetrahedral coordination at the C atom. Using CADPAC,[25] with a standard $8s6p3d$ basis set on C and O, and $6s3p$ on H, distributed multipoles are calculated and shown in Table I. The nomenclature Q_{l0} and Q_{lmc} of Price *et al.*[26] is used. The atom-centered axes are all aligned so that C, O, and H (O) are in the xz plane, the C to O vector defines the positive z direction, and H lies on the positive x side of C and O. The SCF wave function is believed to be fairly close to the Hartree–Fock limit (its expectation energy is $-115.097582E_h$), but the neglect of correlation affects the accuracy of the multipoles somewhat. To compensate, all multipoles are multiplied by 1.063, in order to reproduce the experimental dipole moment of methanol.[27] The intermolecular electrostatic energy is then given by the multipole–multipole interaction tensors tabulated by Price *et al.*,[26] except that dipole–quadrupole and quadrupole–quadrupole interactions are not included; this has a negligible effect on the energy, and saves a considerable amount of computer time. In calculating these quantities and several others which contain the charge density it proved to be necessary to saturate the basis set. Since our resources were limited, we there-

fore chose to use a large basis set at the SCF level rather than to include the correlation at a lower level.

The difference between the multipolar first-order Coulomb energy and the true first-order Coulomb energy is called the penetration energy, because its physical origin is the interpenetration of the diffuse electron clouds around the molecules. The main effect is to reduce the electron–electron repulsion, and the penetration energy is therefore usually negative and depends exponentially on distance, as do the charge densities themselves. Of course, the Pauli principle also operates, leading to repulsion which will be considered below.

The GMUL program[28] is used to calculate the penetration energy. First, the charge density of the molecule is expressed as a sum of Gaussian functions located at the C, O, and H (O) nuclei; this is similar to a Distributed Multipole Analysis,[24] but the spatial extent of the charge density is retained. Then, functional forms describing the Coulomb interaction between these Gaussians are calculated for a range of internuclear separations. This gives the total first-order Coulomb interaction energy. The multipolar energy is then subtracted to give the penetration energy, which is fitted to an appropriate functional form. In practice, only the intermolecular O–H (O) interaction gives significant penetration, because it is the shortest intermolecular contact in the dimer at the energy minimum. The penetration energy is found to consist of a spherically symmetrical O–H (O) contribution, plus an anisotropic correction which depends on the direction of the local x-axis at the hydrogen nucleus [which defines, approximately, the *intramolecular* O–H (O) bond direction]. A fit to the radial dependence of these terms gives

$$E_{\rm pen}=C_0 q_{\rm O} q_{\rm H}\exp(-a_0 R_{\rm OH})/R_{\rm OH} - C_1 q_{\rm O}\mu_{x,{\rm H}}\hat{\mathbf{x}}_H\cdot\hat{\mathbf{R}}_{\rm OH}\exp(-a_1 R_{\rm OH})/R_{\rm OH}^2, \quad (2)$$

where $q_{\rm O}$ and $q_{\rm H}$ are atomic charges Q_{00} (Table I), $\mu_{x,{\rm H}}$ is the Q_{11c} x dipole on H (Table I), $\mathbf{R}_{\rm OH}$ is the intermolecular vector from the O to the H (O) nucleus, $\hat{\mathbf{x}}_H$ is the direction of the local x-axis at the H (O) nucleus, and the parameters are given (in atomic units) by $C_0=43$, $C_1=124$, $a_0=2$, and $a_1=1.4$. Each pair of molecules gives two such contributions, namely O–H (O) and H (O)–O, but in a hydrogen-bonded dimer the pair involved in the hydrogen bond clearly gives much larger penetration than the other pair.

The exchange-repulsion energy arising from the Pauli principle is assumed to be proportional to the charge density overlap integral S_ρ, defined by

$$S_\rho=\int \rho_A^e(\mathbf{r})\rho_B^e(\mathbf{r})d\mathbf{r}, \quad (3)$$

where ρ_A^e and ρ_B^e are the electron densities of the molecules. This approximation has been tested for fluorine, chlorine, and nitrogen dimers[29] with the conclusion that it reproduces the Heitler–London repulsion energy reasonably well (to within 10% or less for a wide range of geometries) when a single proportionality parameter is used. For methanol, the charge density overlap is calculated using GMUL,[28] and fitted to a simple isotropic function $A\exp(-\alpha R)$ between each pair of atoms, where (in atomic units) $A=16.296$ for C–C, 10.382 for C–O, 2.682 for C–H, 22.641 for O–O, and 0.925 for O–H (and zero for H–H); $\alpha=1.82$ for C–C, 1.95 for C–O, 1.86 for C–H, 2.00 for O–O, and 1.88 for O–H. This fits the calculated charge density overlap integrals to within a rms percentage error of 4.7%, which is within the general level of accuracy expected from the overlap model. The proportionality parameter K in the relationship

$$E_{\rm rep}=KS_\rho \quad (4)$$

is chosen to be 6.70 atomic units, as discussed below.

The quantum-mechanical dispersion energy also provides an important contribution to the binding energy between methanol molecules. A reliable value[30] for the C_6 dispersion energy coefficient between methanol molecules is 222.2 atomic units, but its anisotropy is not known. Furthermore, in constructing model potentials for polyatomic molecules, especially molecules with more than one non-hydrogen atom, it is generally accepted that a separate C_6 dispersion energy coefficient should be used for interactions between separate parts of the molecules (atoms or bonds) rather than a single dispersion energy coefficient between molecular centres. Using the published values of $C_6=129.6$ for methane and 45.4 for water dimer,[31] it is reasonable to assign dispersion energy coefficients to the C and O atoms in the methanol molecule, in the same ratio, i.e., C_6(C–C): C_6(O–O)=129.6:45.4, and to use the well-established geometric mean combining rule, $[C_6({\rm C–O})]^2=C_6$ (C–C) C_6(O–O). This gives the chosen C_6 dispersion energy coefficients, in atomic units, as 87.6 for C–C, 30.7 for O–O, and 51.9 for C–O.

The induction, or polarization, energy is the only contribution which has non-additive effects included. The polarizability of the methanol molecule is divided between the C and O atoms (but they are not allowed to polarize each other within the same molecule) and the induction energy for each atom is written as

$$E_{\rm ind}=-(\alpha_{xx}F_x^2+\alpha_{yy}F_y^2+\alpha_{zz}F_z^2)/2, \quad (5)$$

where α is an atomic polarizability and F is the field at the atom due to permanent (distributed) charges and dipoles of other molecules (Table I). Total polarizabilities of the methanol molecule were obtained from CADPAC, in the CHF approximation, and multiplied by 1.136 to reproduce the experimental average polarizability.[27] This gives $\alpha_{xx}=21.5$, $\alpha_{yy}=20.6$, and $\alpha_{zz}=23.8$ atomic units. Atomic polarizabilities are obtained by assuming that $\alpha({\rm C})/\alpha({\rm O})=[C_6({\rm C–C})/C_6({\rm O–O})]^{1/2}$. This gives the values finally used in the potential: $\alpha_{xx}=13.5$ for C and 8.0 for O; $\alpha_{yy}=12.9$ for C and 7.7 for O; $\alpha_{zz}=14.9$ for C and 8.9 for O.

Overall, the potential is therefore a sum of additive electrostatic, penetration, repulsion and dispersion contributions, with a non-additive induction energy. The functional form is most detailed and accurate for the electrostatic energy, which can be calculated most accurately and which is also believed to be the most important in determining the structures and vibrational frequency shifts in the clusters. No explicit intramolecular geometry dependence is included. However,

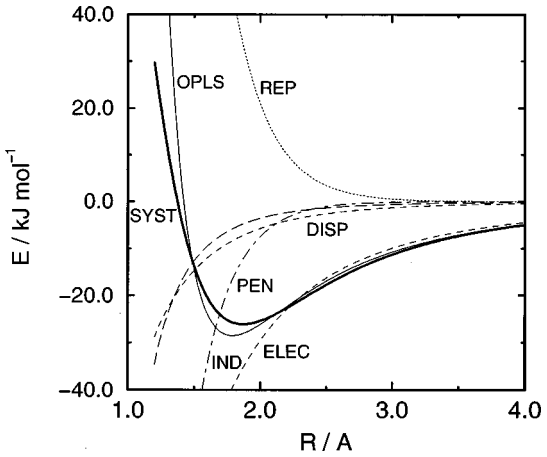

FIG. 1. Components of the methanol potential as a function of the dimer hydrogen bond separation. SYST (thick solid curve) is the systematic intermolecular potential energy, ELEC (short dash curve) is the electrostatic multipole energy, PEN (dot–dash curve) is the penetration energy, REP (dotted curve) is the repulsion energy, IND (long dash curve) is the induction energy, DISP (short dash curve) is the dispersion energy, and OPLS (thin solid curve) is the intermolecular OPLS energy.

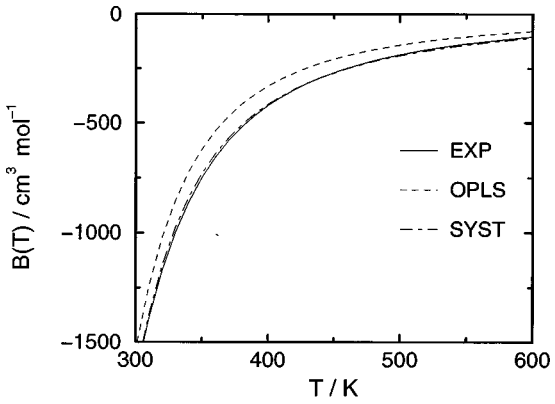

FIG. 2. The second virial coefficients $B(T)$ of methanol vapor. EXP (solid curve) is the experimental curve of Eq. (6) taken from Ref. 32, OPLS (dash curve) is the calculated curve for the OPLS potential taken from Ref. 8, and SYST (dot–dash curve) is the calculated curve for the systematic potential using repulsion parameter $K=6.7$.

since the intermolecular potential is written entirely in terms of atom–atom contributions, there is an implicit dependence on geometry and this can easily be incorporated into a computer program. The only problem is the choice of local axes at each of the nuclei; in practice, these were chosen as described above, with the molecule in the local xz plane, the z axis from C to O and the H (O) atom on the positive x side. Obviously, the multipoles and polarizabilities will change when the intramolecular geometry changes, and this should be built into a more realistic model, but it would be even more important to include effects such as damping of induction and dispersion by charge overlap, anisotropy of the dispersion energy coefficients and of the repulsion parameters, and dispersion energy coefficients higher than C_6.

The separate components of the intermolecular potential are plotted in Fig. 1 as a function of the dimer hydrogen bond separation, while all other intermolecular degrees of freedom are fixed. Furthermore the potential curve of the OPLS model is given. (The steepness of its repulsive part may be attributed to the simple R^{-12} representation, the exaggerated well depth stems from the overestimated dipole moment.) It is noted that SCF calculations for methanol clusters from dimer to hexamer were also performed[21,22] which are discussed elsewhere.[7]

In order to determine the repulsion parameter K of Eq. (4) we have calculated the second virial coefficient $B(T)$ and fitted it to experimental data from measurements of the excess molar enthalpy of methanol–nitrogen.[32] For easy applicability the authors give their values of $B(T)$ over the temperature range 270–700 K in a simple analytical form

$$B(T)=42.581-43.966T_r^{-1}-71.761T_r^{-2}-2.315\exp(3.763T_r^{-1}), \tag{6}$$

where $T_r=T/T^c$ and $T^c=512.64$ K. The curve is plotted in Fig. 2 along with the calculated data for the OPLS potential taken from Ref. 8 and for the new systematic potential. For the calculation of the six dimensional integral,

$$B(T)=-\frac{N_0}{16\pi^2}\int_0^\infty R_B^2 dR_B\int_0^\pi \sin\Theta_B d\Theta_B \times\int_0^{2\pi} d\Phi_B\int_0^{2\pi} d\phi_B \times\int_0^\pi \sin\theta_B d\theta_B\int_0^{2\pi} f(\tau_B)d\psi_B, \tag{7}$$

where N_0 is the Avogadro Number, R_B, Θ_B, Φ_B describe the center of mass position of molecule B in polar coordinates and ϕ_B, θ_B, ψ_B are the Eulerian angles of molecule B, while molecule A may be arbitrarily fixed in space, and $f(\tau_B)$ is the Mayer function,

$$f(\tau_B)=\exp(-V^{int}(\tau_B)/k_bT)-1, \tag{8}$$

where V^{int} is the intermolecular interaction potential, k_B is the Boltzmann constant, and $\tau_B=\{R_B,\Theta_B,\Phi_B,\phi_B,\theta_B,\psi_B\}$; we used a slightly modified program of Evans and Watts.[33]

The integration space is divided into a large number of small hypercubes and for each hypercube a quadrature is performed. The final result is given by the sum over all quadratures of all hypercubes. For each hypercube the integration is split into a Gaussian quadrature with 10 nodes along the R_B coordinate and a quadrature for the five dimensional subspace spanned by Θ_B, Φ_B, ϕ_B, θ_B, ψ_B. Here a non-product second-degree formula is used which is given by Stroud[34] with the exception that Evans and Watts include in addition to the nodes of the five dimensional simplex the center of the corresponding sphere as a further node in their program.

We carefully checked that the arbitrary interval (0,40 a.u.) along coordinate R_B was chosen large enough so that contributions beyond this interval are negligible. Hard-sphere potentials were introduced around the interaction sites (C,O,H) to avoid potential artefacts, but to preserve the an-

TABLE II. Intramolecular force field for methanol. The effective quadratic force constants are denoted by f_{aa}^{eff}. All other values are taken from Ref. 23. Quadratic and cubic bending force constants are given in mdyn Å, quadratic, cubic, and quartic stretching force constants are given in mdyn $Å^{-1}$, mdyn $Å^{-2}$, and mdyn $Å^{-3}$, respectively.

type	OH-str.	CO-str.	COH-bend.
f_{aa}^{eff}	8.2827	5.3431	0.8442
f_{aaa}	−59.8800	−31.8260	−1.4310
f_{aaaa}	420.6690	203.3250	

isotropy of the potential. The final partition of the integration space is given by 12, 6, 12, 12, 6, 12 for R_B, Θ_B, Φ_B, ϕ_B, θ_B, ψ_B, respectively, and the radii of the hard-spheres used in the calculation are $R_C=1.5$ a.u. (C-atom), $R_O=2.5$ a.u. (O-atom), and $R_H=0.5$ a.u. (H-atom of the OH-group). As Fig. 2 illustrates, almost perfect agreement could be achieved between the experimental and the theoretical curve using the systematic potential with a repulsion parameter $K=6.7$. The curve for the OPLS potential illustrates the large overestimation of the binding energy which is caused by the overestimated static dipole moment.

B. Intramolecular potential

Based on the anharmonic SCF force field by Schlegel *et al.*[23] an effective force field is used that takes the hydrogen atoms of the methyl group only implicitly into account.[7] Therefore only force constants for the CO stretch, the OH stretch, and the COH bend coordinates are needed which are listed in Table II. The geometrical parameters of the methanol monomer are the same as given above in the description of the intermolecular potential.

TABLE III. Binding energies E (in kJ/mole), symmetry point group PG, and mean hydrogen bond lengths d (in Å) of the three lowest lying isomers for each cluster size, obtained by means of the systematic intermolecular (a) and its corresponding total cluster potential (b).

M	$-E$	PG	d	$-E'$	PG	d'	$-E''$	PG	d''
				(a)					
2	26.2		1.873	24.9		1.887	24.2		1.901
3	64.9		1.955	63.3	C_3	1.966	61.3		1.861
4	125.1	S_4	1.774	122.1	C_i	1.785	109.4		1.770
5	174.7		1.726	159.9		1.737	153.1		1.763
6	221.3	S_6	1.710	217.7	C_2	1.717	207.9		1.750
7	260.5		1.713	258.0		1.713	257.8		1.716
8	303.8	S_4	1.718	301.8	S_8	1.712	301.8	C_i	1.711
9	345.4		1.705	338.9		1.713	337.6		1.730
10	391.4		1.720	390.0		1.710	388.1	C_i	1.702
				(b)					
2	26.8		1.849						
3	67.0		1.923	65.4	C_3	1.934	63.4		1.823
4	132.0	S_4	1.713	128.8	C_i	1.726	114.6		1.715
5	186.7		1.645				161.6		1.696
6	238.0	S_6	1.617	233.8	C_2	1.628	222.0		1.669
7	280.7		1.618				277.4		1.624
8	325.8	S_8	1.614	324.0	S_4	1.627	323.6	C_i	1.624
9	371.1		1.605	365.9		1.615	359.9		1.644
10	418.5		1.609	417.8	C_i	1.600	417.0		1.636

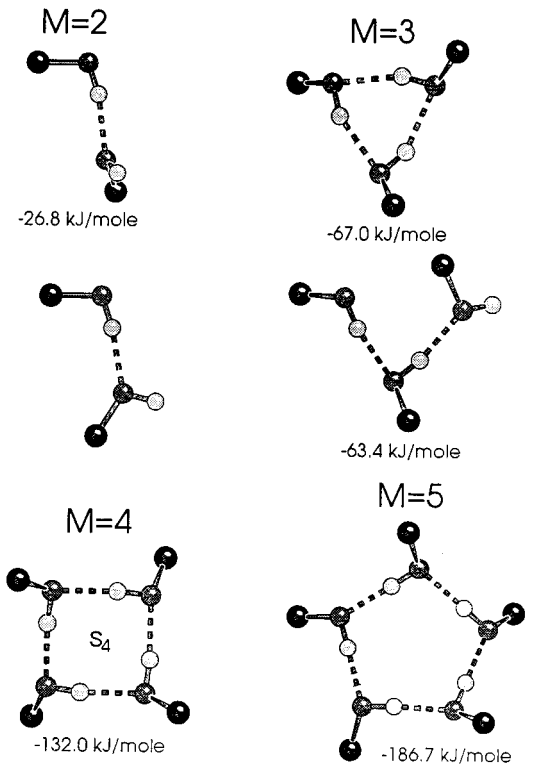

FIG. 3. The energetically most stable methanol structures from dimer to pentamer for the systematic total cluster potential. The numbers indicate the energies of the minima. The second panel illustrates a planar dimer configuration which is unstable with respect to the total cluster PES, and the energetically most stable trimer chain structure.

III. STRUCTURE CALCULATIONS

Following the *cluster approach* we determine cluster structures in a stepwise procedure. First we calculate minima on the intermolecular potential energy surface (PES), where the molecules are kept rigid. This reduces the dimension of the configurational space drastically and therefore saves a lot of computer time while preserving the most important features of the total cluster potential that determine the structure. Local minimum configurations serve as input for the total cluster PES and are further minimized in a second step with respect to all internal cluster coordinates. Usually only minor configurational changes occur during the second minimization step. However, some cluster configurations may be unstable and disappear, while others may be distorted in an unphysical way. Unstable structures are interesting, since their disappearance may change the interpretation of an experimental spectrum. Unphysical distortion of structures merely indicates the breakdown of the potential ansatz which did not happen in our calculations using the systematic potential.

The results of our configuration calculations with the systematic potential are summarized in Table III and Figs. 3, 4, 5. Table III shows the binding energies, the symmetries, and the mean hydrogen bond lengths for the three lowest lying isomers of each methanol cluster size, ranging from dimer to decamer. In panel (a) the results were obtained using only the systematic potential, in panel (b) the combined

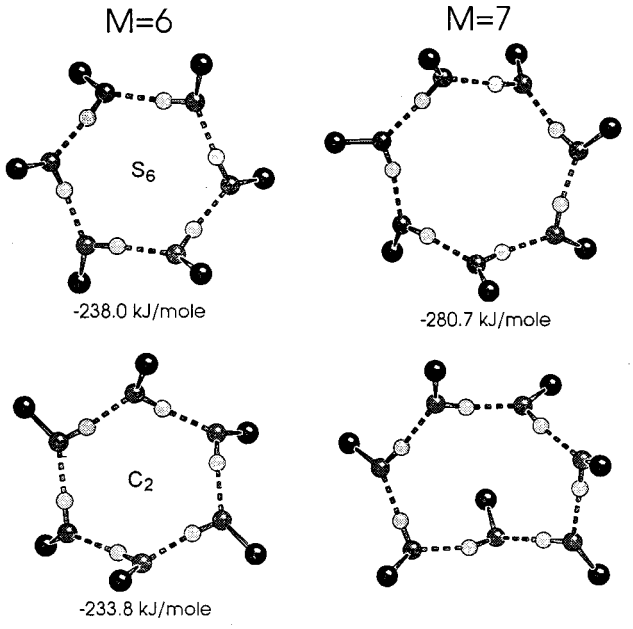

FIG. 4. The first panel shows the energetically most stable hexamer and heptamer structures, the second panel illustrates the second lowest hexamer structure and a heptamer configuration which is unstable with respect to the systematic total cluster PES. The numbers indicate the energies of the minima.

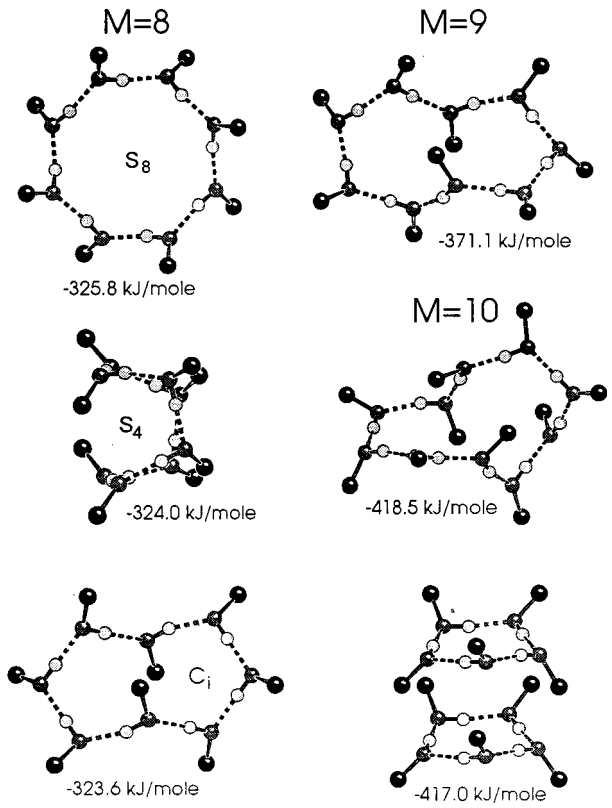

FIG. 5. The three energetically most stable octamer structures, the lowest nonamer structure, and the lowest and third lowest decamer structure for the systematic total cluster potential. The numbers indicate the energies of the minima.

intra-intermolecular potential was used. Note that some of the configurations vanish in panel (b) which means that the input configurations obtained with the systematic potential are not stable on the total cluster PES. Especially for the second and third lowest energy dimer configurations this is a reasonable result because both structures are planar so that no linear hydrogen bond can be uniquely defined as is illustrated for the second lowest dimer configuration in Fig. 3.

It is well known that the hydrogen bond determines the structure of methanol clusters as well as that of the bulk material. In the solid α-phase long chains are formed with the C-atoms alternately pointing up and down.[35] This can easily be understood in terms of the tetrahedral structure of the sp^3-orbitals of the O-atoms which, indeed, determines the structure of the linear hydrogen bond. Free lone pair electron clouds repel each other and maximize their distance so that as a consequence the C-atoms are alternately pointing up and down.

To maximize their binding energy free clusters will maximize their number of hydrogen bonds. Therefore we expect ring structures for clusters with more than two molecules instead of linear structures. For clusters with an even number of molecules the up and down pattern can be perfectly preserved (as can be illustrated with the simple string pattern udud) and leads to structures with S_{2M} symmetry, $M=2,3,4$.

For clusters with an odd number of molecules the up and down pattern cannot be preserved so that a distorted ring configuration is formed, where one molecule is almost in the ring plane. We shall call the acceptor hydrogen bond of this molecule the closure point of the odd-numbered ring configuration.

As can be seen in Figs. 3, 4, and 5 only the lowest energy dimer configuration has a well defined (proton) donor molecule and an acceptor molecule since in ring configurations all molecules are both the donor and the acceptor at the same time. The mean hydrogen bond lengths of the most stable structures decrease monotonically from trimer with 1.923 Å for the total cluster potential to hexamer with 1.617 Å. However, from a dimer (1.849 Å) to a trimer (1.923 Å) a large increase is observed. This property can be attributed to the structural change from the dimer chain configuration to the ring structure of the trimer. As expected the additional hydrogen bond in the trimer configuration energetically overcompensates the energy that is needed for the deformation of the hydrogen bond from linear. This deformation can be further characterized by another geometrical parameter α which measures the planarity of a ring configuration,

$$\alpha = \left| \arccos\left(\frac{\mathbf{e}_{\mathrm{OH}}^{i \bmod M} \times \mathbf{e}_{\mathrm{OH}}^{(i+1) \bmod M}}{\left| \mathbf{e}_{\mathrm{OH}}^{i \bmod M} \times \mathbf{e}_{\mathrm{OH}}^{(i+1) \bmod M} \right|} \cdot \frac{\mathbf{e}_{\mathrm{OH}}^{i \bmod M} \times \mathbf{e}_{\mathrm{OH}}^{(i-1) \bmod M}}{\left| \mathbf{e}_{\mathrm{OH}}^{i \bmod M} \times \mathbf{e}_{\mathrm{OH}}^{(i-1) \bmod M} \right|} \right) \right|, \quad i = 2, \ldots, M+1, \tag{9}$$

where $\mathbf{e}_{\mathrm{OH}}^{i \bmod M}$ is the unit vector of molecule i pointing from the oxygen atom to the hydrogen atom. The value of α is

TABLE IV. Geometry parameter α of Eq. (9) for the lowest energy ring configurations from trimer to octamer for the systematic and the OPLS total cluster PES.

	Angle/deg						
	Systematic				OPLS		
M	PG	$\overline{\alpha}$	α_{min}	α_{max}	PG	$\overline{\alpha}$	α_{min}	α_{max}
3		4.8	4.7	4.9	C_{3h}	0.0	0.0	0.0
4	S_4	19.5	19.5	19.5	C_{4h}	0.0	0.0	0.0
5		24.1	2.8	36.7		16.9	3.5	26.1
6	S_6	50.6	50.6	50.6	S_6	42.4	42.4	42.4
7		58.6	30.1	76.2				
8	S_8	80.4	80.4	80.4				

equal to zero for a planar ring configuration. The average and the min/max values of α for the most stable ring structures of the total systematic and OPLS potential are listed in Table IV.

The data for the trimer configuration show that it is almost planar as concerns the $\mathbf{e}_{\mathrm{OH}}^{i\mathrm{mod}M}$ unit vectors. Therefore the sp^3-orbitals of the oxygen atoms are quite distorted which explains the large hydrogen bond separation. The average of α increases from the trimer to the octamer which indicates that the hydrogen bonds become more and more relaxed. On the other hand this means that there will be an increasing tendency to deviate from the above described building pattern for the most stable structures. A large difference is found between the minimal and the maximal value of α for the pentamer and the heptamer. The smaller value can easily be attributed to the closure point of a cluster with an odd number of molecules. In Figs. 3 and 4 the molecules on the left hand side of pentamer and heptamer lie at the closure point of the cluster. For the OPLS potential it is shown in Table IV that it lacks a sufficient description of the anisotropic features of the true intermolecular methanol interaction.

Although the most stable ring structures of the total cluster potential from the trimer to the octamer deviate somewhat from planarity this is an important feature of these configurations which we call quasi planarity in the further course of this paper. The first distinct deviation from quasi planarity is found for the second lowest energy configuration of the heptamer using only the intermolecular potential. One molecule in the cluster which is shown in Fig. 4 flips down so that aside from the almost regular up/down pattern two dimer configurations can be observed within the ring (the lower three molecules of the cluster). This structure is unstable, however, with respect to the total cluster PES. A similar behavior is found for the energetically second and third lowest octamer configurations and for the lowest nonamer and decamer configurations shown in Fig. 5. In all these cases two flips occur, where the flipped molecules face each other on the other side of the ring.

In Fig. 5 the third lowest energy configuration of the decamer indicates another structural change. It consists of two sandwiched pentamers and has the same number of hydrogen bonds as the large decamer ring of Fig. 5.

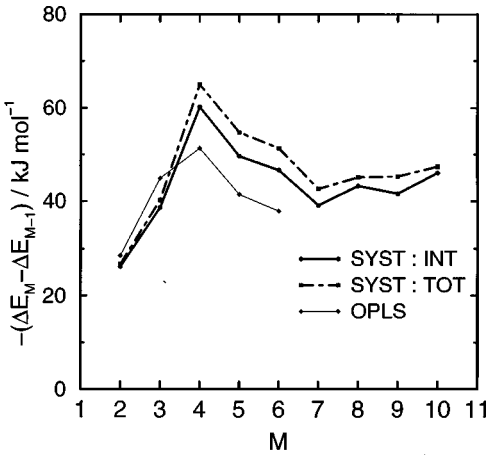

FIG. 6. Incremental binding energies of methanol clusters from dimer to decamer for the intermolecular systematic potential (SYST:INT), the systematic total cluster PES (SYST:TOT), and the intermolecular OPLS potential.

The incremental binding energies $-(\Delta E_M - \Delta E_{M-1})$ as a function of M are plotted in Fig. 6 for the intermolecular and the total systematic potential and for the intermolecular OPLS potential taken from Ref. 8. A pronounced peak is found for $M=4$ which may be caused by the cooperativity effect. To check this we looked at the different contributions V^{elec}, V^{pen}, V^{rep}, V^{ind}, and V^{disp} to the intermolecular binding energy V^{int} which are listed in Table V for the lowest energy configurations up to the tetramer. The relative increase of the induction energy is, indeed, the largest of all potential components. However, its contribution to the overall binding energy is so small that the optimization of the pairwise additive components plays also a major role. This idea is corroborated by the fact that the OPLS potential gives the correct peak at $M=4$ without including any non-additive part. The large increase in the incremental binding energy from dimer to trimer for the OPLS potential can be understood in terms of the gain of symmetry which is not realistic, however.

IV. CLUSTER APPROACH

The first step in applying the cluster approach is to construct a total cluster potential from separated intra- and intermolecular interaction models. Taking into account that the interaction sites of the intra- and intermolecular potential of Sec. IV correspond to three atomic sites of the methanol molecule we may write

TABLE V. Contributions of the repulsion, multipole, penetration, dispersion, and induction energy to the intermolecular binding energy of the lowest energy dimer, trimer, and tetramer configurations in kJ/mole.

M	V^{rep}	V^{mult}	V^{pen}	V^{disp}	V^{ind}	V^{int}
2	33.2	−35.2	−12.2	−7.2	−4.8	−26.2
3	79.4	−89.9	−25.1	−17.0	−12.3	−64.9
4	188.7	−175.4	−69.7	−33.1	−35.6	−125.1

$$V^{tot}=\sum_{m}^{M}\left(\sum_{a}^{9}\sum_{b<a}^{9}v_{ab}^{m}(R_a^m,R_b^m)+\sum_{a}^{9}\sum_{b<a}^{9}\sum_{c<b}^{9}v_{abc}^{m}(R_a^m,R_b^m,R_c^m)+\ldots\right)+\sum_{m}^{M}\sum_{n<m}^{M}\left(\sum_{a}^{9}\sum_{b}^{9}v_{ab}^{mn}(R_a^m,R_b^n)+\ldots\right)+\sum_{m}^{M}\sum_{n<m}^{M}\sum_{o<n}^{M}\left(\sum_{a}^{9}\sum_{b}^{9}\sum_{c}^{9}v_{abc}^{mno}(R_a^m,R_b^n,R_c^o)+\ldots\right)+\ldots \tag{10}$$

for the total interaction energy.[7] Here, the expression in the first two lines represents the M intramolecular force fields and the other three lines are molecular two- and three-body interactions expressed by atomic two- and three-body interactions. The $3M$ boundary conditions $R_a^m-{}^0R_a^m=0$, $a=1,2,3$, $m=1,\ldots,M$, where ${}^0R_a^m$ is the position of atom a in molecule m, are lifted so that intra- and intermolecular interactions are coupled.

A. Harmonic approximation

Having calculated minima on the total cluster potential energy surface the potential is expanded into a series around the minimum configurations in mass-weighted Cartesian coordinates $d_i=\sqrt{m_i}(x_i-x_i^0)$, $i=1,\ldots,3N$, where N is the number of atoms in the cluster. Note that all carbon atoms are given an effective mass of 15 u since the hydrogen atoms of the methyl group have to be taken into account. The quadratic force constant matrix $(\partial^2V^{tot}/\partial d_i\partial d_j)_{i,j}$ is calculated and diagonalized numerically.[7]

B. Anharmonic corrections

Our total cluster Hamiltonian may be written as

$$H=\sum_{m=1}^{M}\left(\frac{1}{2}\sum_{a=1}^{9}\omega_{a,m}(p_{a,m}^2+q_{a,m}^2)\right)+\sum_{m,n,o=1}^{M}\left(\frac{1}{6}\sum_{a=1}^{9}\sum_{b=1}^{9}\sum_{c=1}^{9}\phi_{abc,mno}q_{a,m}q_{b,n}q_{c,o}\right)+\sum_{m,n=1}^{M}\left(\frac{1}{24}\sum_{a=1}^{9}\sum_{b=1}^{9}\phi_{aabb,mn}q_{a,m}^2q_{b,n}^2\right)+\sum_{\alpha}B_\alpha\pi_\alpha^2, \tag{11}$$

where the first sum describes the intramolecular harmonic oscillations which are coupled to the intermolecular modes in the minimization procedure of the total interaction energy [see Eq. (10)]. The other terms represent the anharmonic corrections. $q_{a,m}$ and $p_{a,m}$ are dimensionless normal coordinate and momentum operators, $\omega_{a,m}$ are harmonic frequencies, $\phi_{abc,mno}$ and $\phi_{aabb,mn}$ are cubic and quartic force constants, B_α are the usual rotational constants, and π_α are the vibrational angular momenta.[36] Only in the calculation of the vibrational angular momenta the intermolecular modes are explicitly taken into account.

The anharmonic correction may be taken into account via non-degenerate second-order perturbation theory which yields for the vibrational energy levels,

$$E(\mathbf{v})=\sum_i\omega_i\left(v_i+\frac{1}{2}\right)+\sum_{i\geqslant j}\chi_{ij}\left(v_i+\frac{1}{2}\right)\left(v_j+\frac{1}{2}\right)+\ldots, \tag{12}$$

where χ_{ij} are the anharmonicity constants.[37] Note that even for symmetric top clusters this formula may be used as long as algorithms are employed for the diagonalization of the quadratic force constant matrix $(\partial^2V^{tot}/\partial d_i\partial d_j)_{i,j}$ which produce an orthogonal transformation matrix $\mathbf{l}$ so that $\mathbf{l}^T\mathbf{F}\,\mathbf{l}=\mathrm{diag}(\lambda_1,\ldots,\lambda_{3N-6})$.

The linear variational ansatz is another standard method to take anharmonicity into account. We used it for the cubic and quartic force constant contributions but left the rotational contribution for a perturbational calculation. To reduce the dimensionality of the variational matrix for each mode of interest $\omega_{u,v}$ we set up a simplified Hamiltonian,

$$H^{var}=\tfrac{1}{2}\omega_{u,v}(p_{u,v}^2+q_{u,v}^2)+\sum_{n,o=1}^{M}\left(\frac{1}{6}\sum_{b=1}^{3}\sum_{c=1}^{3}\phi_{ubc,vno}q_{u,v}q_{b,n}q_{c,o}\right)+\sum_{n=1}^{M}\left(\frac{1}{24}\sum_{b=1}^{3}\phi_{uubb,vn}q_{u,v}^2q_{b,n}^2\right). \tag{13}$$

All diagonal matrix elements $\langle v_{u,v}v_{b,n}|H^{var}|v_{u,v}v_{b,n}\rangle$, $(b\neq u\wedge n\neq v)$ and $\langle v_{u,v}v_{b,n}=1\,v_{c,o}=1|H^{var}|v_{u,v}v_{b,n}=1\,v_{c,o}=1\rangle$, $(b\neq u\wedge n\neq v, c\neq u\wedge o\neq v, c\neq b\wedge o\neq n)$ were taken into account and their corresponding off-diagonal terms. For all quantum numbers $v_{\ldots}$ the unequality $v_{\ldots}\leqslant 4$ holds. Therefore the dimensionality of the Hamiltonian matrix which has to be diagonalized is given by $\mathcal{N}=(45M^2+75M)/2-10$.

C. Infrared intensities

In the harmonic approximation the infrared intensities of a fundamental excitation are proportional to $\langle v_{u,v}=1|\boldsymbol{\mu}_{\textbf{cluster}}|v_{u,v}=0\rangle$, where $\boldsymbol{\mu}_{\textbf{cluster}}$ is the dipole moment operator as a function of normal coordinates. Under the assumption that the charges c_i on the atomic sites do not vary much for small deviations from their original positions we have

$$\langle v_{u,v}=1|\boldsymbol{\mu}_{\textbf{cluster}}|v_{u,v}=0\rangle=\frac{1}{\sqrt{2}}\sum_{\alpha=x,y,z}\sum_{i=1}^{N}\frac{\partial\mu_{cluster}^{\alpha}}{\partial d_{i\alpha}}\frac{\partial d_{i\alpha}}{\partial q_{u,v}}\,\mathbf{e}_\alpha, \tag{14}$$

which is easily calculated numerically. In the following discussion only relative intensities for each mode of interest are given.

TABLE VI. Frequency shifts (cm^{-1}) for the lowest energy configurations from dimer to octamer for the CO stretch mode (1033.5 cm^{-1}) and the OH stretch mode (3681.5 cm^{-1}) in the harmonic approximation (C1) and the anharmonic approximation using a perturbational calculation (C2) and a variational calculation (C3). Relative intensities are given in the harmonic approximation in brackets. S is the symmetry. The experimental data for the CO stretch mode are taken from Ref. 6 and for the OH stretch mode from Refs. 16, 18.

	CO str.					OH str.				
M	Exp	S	C1	C2	C3	Exp	S	C1	C2	C3
2	−7	*a*	−12(0.49)	−7	−7	3	a	−40(0.48)	−26	17
	19	*a*	16(0.51)	20	20	−107	a	−162(0.52)	−146	−131
3	8	*a*	3(0.39)	5	6	−172	a	−187(0.46)	−163	−135
		a	5(0.31)	7	9	−211	a	−194(0.46)	−171	−178
		a	8(0.30)	10	11	−248	a	−225(0.08)	−200	−213
4	11	*b*	3(0.40)	5	8		b	−303(0.11)	−264	
		e	8(0.60)	10	13		e	−323(0.89)	−281	
5	14	*a*	4(0.31)	11	14		a	−356(0.09)	−303	
		a	7(0.07)	10	12		a	−366(0.12)	−314	
		a	10(0.18)	14	15		a	−386(0.36)	−329	
		a	14(0.26)	18	21		a	−394(0.36)	−336	
		a	16(0.18)	21	22		a	−429(0.07)	−362	
6	7	a_u	3(0.31)	13	15		a_u	−387(0.17)	−347	
	19	e_u	20(0.69)	26	29		e_u	−426(0.83)	−376	
7		*a*	−6(0.08)	6			a	−379(0.08)	−326	
		a	3(0.27)	21			a	−386(0.15)	−339	
		a	4(0.06)	20			a	−396(0.05)	−351	
		a	6(0.04)	19			a	−402(0.04)	−353	
		a	10(0.06)	20			a	−427(0.30)	−371	
		a	13(0.16)	27			a	−428(0.32)	−371	
		a	20(0.33)	33			a	−455(0.06)	−392	
8		*b*	2(0.28)	24			*b*	−386(0.21)	−338	
		e_1	21(0.72)	33			e_1	−434(0.79)	−355	

V. FREQUENCY SHIFTS

We have calculated frequency shifts for the CO stretch and the OH stretch mode with respect to the monomer values at 1033.5 cm^{-1} for the CO stretch and 3681.5 cm^{-1} for the OH stretch mode using all three approximations described in Sec. IV. The results are listed for the lowest energy configurations from dimer to octamer in Table VI, for the second and third lowest structures of hexamer and octamer in Table VII, for nonamer and decamer in Table VIII, and for the lowest chain structures from dimer to tetramer in Table IX. Note that in this section binding energies of clusters are always given with respect to the total cluster potential. C1, C2, and C3 in Tables VI–IX denote frequency shifts calculated in the harmonic and the anharmonic approximation using a perturbational and a variational calculation, respectively.

For the CO stretch mode for $M=2-6$ the results of the variational calculation for the lowest energy configurations are illustrated as stick spectra within measured spectra of size selected methanol clusters[6] in Fig. 7. An analogous comparison with experimental results for the OH stretch mode[16,18] for dimer and trimer is shown in Fig. 8. Note that the frequency shifts only are results of a variational calculation, while the relative intensities are given in the harmonic approximation.

For the CO stretch mode in Fig. 7 a very good agreement between theoretical and experimental results is found up to the tetramer. The results listed in Table VI show that for the dimer already in the harmonic approximation an almost correct line splitting is calculated, however, that the overall position of the two resonances is shifted by about 5 cm^{-1} to the red. Both anharmonic approximations yield exactly the same correction and even for larger clusters there are only minor differences between the results of the two approaches. There-

TABLE VII. Frequency shifts (cm^{-1}) for the energetically second lowest hexamer configuration and for the second and third lowest octamer configurations for the CO stretch mode (1033.5 cm^{-1}) and the OH stretch mode (3681.5 cm^{-1}) in the harmonic approximation (C1) and the anharmonic approximation using a perturbational calculation (C2) and a variational calculation (C3). Relative intensities are given in the harmonic approximation in brackets. *S* is the symmetry.

		CO str.				OH str.		
M	*PG*	*S*	C1	C2	C3	*S*	C1	C2
6	C_2	*a*	5(0.31)	7	9	*a*	−375(0.13)	−321
		a	10(0.08)	14	17	*a*	−388(0.09)	−329
		a	13(0.06)	19	19	*a*	−445(0.00)	−371
		b	4(0.09)	8	12	*b*	−372(0.09)	−317
		b	8(0.17)	13	17	*b*	−405(0.34)	−345
		b	16(0.29)	20	24	*b*	−420(0.35)	−351
8	S_4	*b*	−14(0.13)	5		*b*	−363(0.30)	−323
		b	12(0.22)	21		*b*	−458(0.06)	−470
		e	−13(0.21)	4		*e*	−366(0.17)	−331
		e	11(0.44)	19		*e*	−463(0.47)	−468
8	C_i	a_u	−10(0.22)	−7		a_u	−352(0.23)	−303
		a_u	10(0.22)	15		a_u	−400(0.19)	−336
		a_u	11(0.27)	13		a_u	−432(0.29)	−355
		a_u	22(0.30)	27		a_u	−458(0.29)	−346

TABLE VIII. Frequency shifts (cm^{-1}) for the energetically lowest nonamer configuration and for the lowest and second lowest decamer configurations for the CO stretch mode (1033.5 cm^{-1}) and the OH stretch mode (3681.5 cm^{-1}) in the harmonic approximation (C1) and the anharmonic approximation using a perturbational calculation (C2). Relative intensities are given in the harmonic approximation in brackets. E is the binding energy in kJ/mole.

		CO str.				OH str.			
M	$-E$	C1	C1	C2	C2	C1	C1	C2	C2
9	345.4	−2(0.09)	10(0.16)	6	21	−376(0.10)	−443(0.11)	−324	−385
		−10(0.08)	10(0.10)	2	16	−382(0.10)	−458(0.20)	−321	−377
		−15(0.09)	19(0.14)	−2	24	−411(0.06)	−477(0.17)	−373	−396
		7(0.12)	20(0.16)	12	28	−416(0.09)	−486(0.06)	−351	−430
		8(0.07)		12		−430(0.11)		−377	
10	391.4	0(0.16)	7(0.06)	3	8	−339(0.10)	−393(0.08)	−300	−338
		−3(0.04)	8(0.16)	1	12	−343(0.08)	−444(0.13)	−303	−470
		−7(0.04)	8(0.06)	0	13	−369(0.10)	−444(0.12)	−338	−471
		−11(0.11)	11(0.12)	5	15	−371(0.10)	−476(0.11)	−337	−483
		−14(0.12)	11(0.14)	1	13	−387(0.16)	−480(0.04)	−340	−482
10	390.0	−7(0.11)	8(0.12)	17	18	−357(0.10)	−439(0.06)	−307	−371
		−9(0.05)	10(0.07)	11	16	−365(0.08)	−453(0.09)	−311	−432
		−12(0.10)	11(0.07)	8	20	−390(0.08)	−463(0.11)	−336	−416
		−18(0.12)	13(0.09)	−1	22	−407(0.09)	−483(0.14)	−369	−454
		5(0.16)	15(0.09)	13	22	−423(0.14)	−524(0.10)	−360	−435

fore we can easily conclude that the Hamiltonian of Eq. (13) gives the major contribution to the vibrational energy states and that no Fermi and/or Darling–Dennison resonance leads to a (partial) breakdown of the perturbational ansatz. For trimer and tetramer the anharmonic correction again mainly consists of a small overall blueshift, for pentamer and hexamer the overall blueshift exceeds the experimental result by 3 cm^{-1} and 10 cm^{-1}, respectively. Aside from these shifts, the distances between the lines for the pentamer and hexamer are reduced which results in a much better agreement with experiment.

Figure 8 shows a surprising good agreement between the experimental peak positions for the OH stretch mode for dimer and trimer and marks indicating the frequency shifts in the variational approximation. Note that for the trimer the calculated values are shifted by 35 cm^{-1}. We do not illustrate the harmonic intensities in this figure, because we are

TABLE IX. Frequency shifts (cm^{-1}) for the energetically lowest chain structures from dimer to tetramer for the CO stretch mode (1033.5 cm^{-1}) and the OH stretch mode (3681.5 cm^{-1}) in the harmonic approximation (C1) and the anharmonic approximation using a perturbational calculation (C2). Relative intensities are given in the harmonic approximation in brackets. E is the binding energy in kJ/mole.

		CO str.		OH str.	
M	$-E$	C1	C2	C1	C2
2	26.8	−12(0.49)	−7	−40(0.48)	−26
		16(0.51)	20	−162(0.52)	−146
3	63.4	−32(0.29)	−29	−31(0.32)	−27
		5(0.38)	7	−202(0.37)	−177
		18(0.33)	21	−233(0.31)	−206
4	114.6	−34(0.23)	−31	−37(0.24)	−33
		4(0.33)	6	−281(0.23)	−247
		8(0.22)	10	−287(0.28)	−300
		21(0.22)	10	−341(0.25)	−300

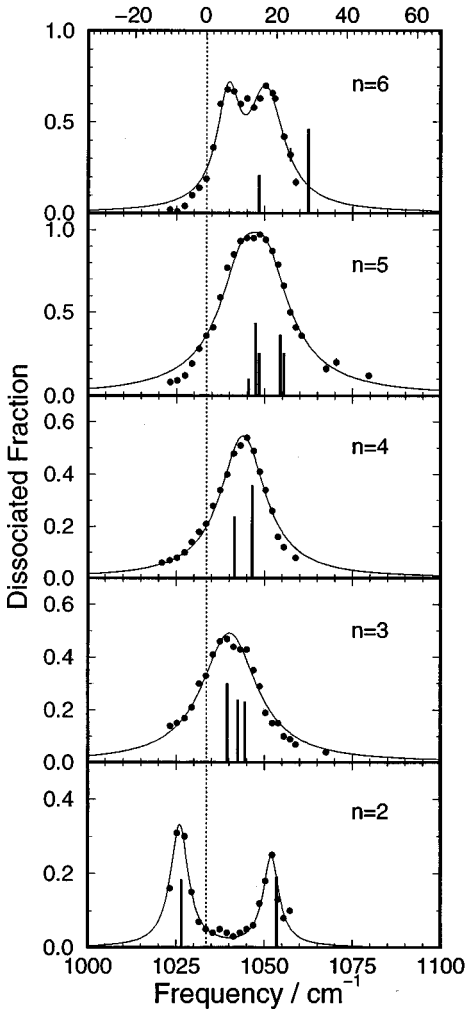

FIG. 7. Comparison of experimental data taken from Ref. 6 with theoretical lineshift calculations in the variational approximation from dimer to hexamer for the CO stretch mode. The dotted line indicates the monomer value at 1033.5 cm^{-1}. The upper abscissa denotes line shifts with respect to the monomer value while the lower abscissa gives the absolute values.

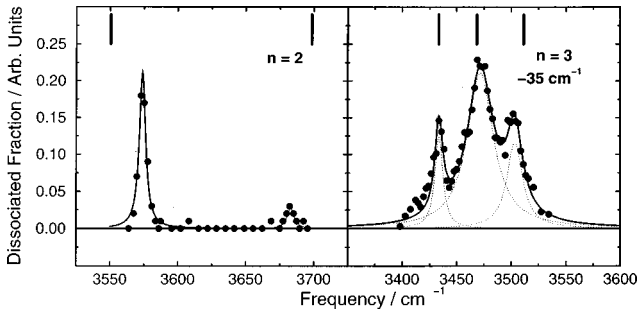

FIG. 8. Comparison of experimental data taken from Refs. 16–18 with theoretical lineshift calculations in the variational approximation for dimer and trimer for the OH stretch mode. Note that for the trimer the calculated values are shifted by 35 cm^{-1}.

convinced that for these modes the harmonic approximation is not sufficient anymore. As listed in Table VI the anharmonic contributions are large and in addition to this there are distinct differences between the perturbational and the variational results. Especially for the trimer only the variational calculation yields line shifts which are satisfactorily in agreement with the experimental evidence. The harmonic and the perturbation approach both yield two lines which are separated by less than 10 cm^{-1} and a third line which is located about 30 cm^{-1} to the red relative to the two narrow lying resonances. This may be understood in terms of quasiplanarity described in Sec. III. Since the intramolecular OH bonds lie almost in a plane and the OH stretch modes are strongly localized in these bonds we find an approximate C_{3h} symmetry like behavior. Therefore the quasi degeneracy of the two narrow lying resonances and their strong (harmonic) relative intensity amounting to 92% and the approximate infrared inactivity of the third mode may well be understood. The variational results, however, need a more thorough discussion which we give below. Note that the argument of quasi degeneracy is not applicable to the CO stretch modes since the CO bonds are pointing up and down relative to the symmetry plane.

The results for the lowest energy heptamer and octamer structures in Table VI are compared with experimental results for CO and OH stretch modes in a subsequent paper.[19] Note, however, that the results for the relative intensities of the OH stretch modes of the heptamer again indicate an approximate C_{7h} symmetry like behavior. Because of the S_8 symmetry of the octamer only two infrared active modes are calculated for CO and OH stretch modes. In the harmonic approximation the results for the CO stretch mode are quite similar to those obtained for the hexamer. But in the anharmonic approximation using perturbation theory the overall blueshift obtained for the octamer exceeds that obtained for the hexamer by about 10 cm^{-1}.

In Table VII we have listed the line shifts of the second lowest energy hexamer configuration with C_2 symmetry and of the second and third lowest energy configurations of the octamer with S_4 and C_i symmetry, respectively. This is interesting as attempts were undertaken to induce structural transitions in size-selected methanol hexamers[38] using the

TABLE X. Harmonic frequencies and important cubic and quartic force constants for the OH stretch modes of the lowest energy trimer configuration.

Force constants, cm^{-1}		
$\omega_1=3665$	$\omega_2=3658$	$\omega_3=3627$
$\phi_{111}=-1596$	$\phi_{222}=-134$	$\phi_{333}=-1571$
$\phi_{1111}=1267$	$\phi_{2222}=984$	$\phi_{3333}=726$
$\phi_{112}=348$	$\phi_{221}=809$	$\phi_{311}=-1299$
$\phi_{113}=-1299$	$\phi_{223}=-1644$	$\phi_{322}=-1644$
$\phi_{1133}=503$	$\phi_{2233}=794$	$\phi_{3311}=503$
		$\phi_{3322}=794$

spectroscopic fingerprints to identify the participating configurations. Both octamer configurations have four infrared active CO and OH stretch modes. In the harmonic approximation two CO stretch modes of the S_4 configuration are shifted to the red, while only blueshifts are obtained using the perturbational calculation. For the octamer with C_i symmetry in both approximations a redshifted CO stretch mode is calculated. In Table VIII the results for the lowest energy nonamer and the two lowest energy decamer structures are listed. Since these structures are not symmetric their spectra are quite complicated and it will be difficult to identify specific configurations by comparing them to low resolution spectra.

A very specific behavior of acceptor modes is obtained for chain structures for which we list the results of our frequency shift calculations in Table IX. For each chain structure only one CO stretch mode is shifted to the red which may be unambiguously attributed to the acceptor molecule. Only one OH stretch mode is shifted to the red by less than 40 cm^{-1} which again may be unambiguously attributed to the acceptor molecule. This unique feature allows us to easily identify chain structures in molecular beam experiments.

For all lowest energy configurations we have examined the most important cubic and quartic force constants which contribute to the lineshift calculations in the perturbational approximation. This gives interesting insight into the nature of a specific frequency shift. As an example we would like to discuss the force constants of the OH stretch modes of the lowest energy trimer configuration which has an approximate C_{3h} symmetry. The force constants are listed in Table X and we begin with the discussion of the two quasi degenerate modes $\omega_1=3665$ cm^{-1} and $\omega_2=3658$ cm^{-1}. Since $\Gamma(e')\otimes\Gamma(e')\otimes\Gamma(e')=3\Gamma(e')\oplus 2\Gamma(a')$ and $\phi_{111}=1596$ cm^{-1} is a large contribution, we conclude that the quasi degenerate pair of modes ω_1 and ω_2 has e' symmetry. A different conclusion is drawn, however, if we look at the force constants of mode ω_2. Since $\Gamma(e'')\otimes\Gamma(e'')\otimes\Gamma(e'')=3\Gamma(e'')\oplus 2\Gamma(a'')$ and ϕ_{222} is small we would now assign the e'' symmetry to the quasi degenerate modes. The only solution to this problem is that, indeed, the two modes have different approximate symmetries. This picture holds, if we note that $\phi_{221}=809$ cm^{-1} considerably contributes to the anharmonicity ($\Gamma(e'')\otimes\Gamma(e'')\otimes\Gamma(e')=3\Gamma(e')\oplus 2\Gamma(a')$), but that the coupling constant ϕ_{112} is small and negligible ($\Gamma(e')\otimes\Gamma(e')\otimes\Gamma(e'')=3\Gamma(e'')\oplus 2\Gamma(a'')$). The a'' symmetry is

easily attributed to mode $\omega_3 = 3627\ \mathrm{cm}^{-1}$ and no further discussion is needed for this mode. One of the most remarkable results of the lineshift calculations for the trimer, however, is the difference obtained for the perturbational and the variational approach. This can hardly be understood in terms of an approximate C_{3h} symmetry, if we exclusively attribute e' or e'' symmetry to modes ω_1 and ω_2, since the two modes would couple directly. Recognizing, however, that the two modes have different symmetry, we easily see that direct coupling is impossible. On the other hand, the two modes are almost resonant so that we would expect coupling via $\phi_{1122} = 228\ \mathrm{cm}^{-1}$. The matrix element $\langle v_1 = 2 v_2 = 0 | \phi_{1122} | v_1 = 0 v_2 = 2 \rangle$, however, is only included in the variational calculation and may well be responsible for the line splitting of the two quasi degenerate modes.

Inspection of the most important force constants of the infrared active degenerate CO stretch modes of the lowest energy ring configurations with S_M symmetry revealed that these modes are strongly coupled to the OH stretch modes of the cluster. The coupling of the infrared active a_u modes, however, is negligible. Therefore, problems in the description of the OH modes will probably produce problems in the description of the degenerate CO stretch modes with e_u symmetry.

VI. DISCUSSION

Based on a new systematic intermolecular potential results of structure and frequency shift calculations are reported in this paper. Special care has been taken for a detailed description of the electrostatic interaction using a distributed multipole representation and a penetration term. Aside from that the potential consists of a repulsion, dispersion, and non-additive induction terms. As it is constructed mainly from properties of SCF monomer wave functions, it is suited for the description of the interaction energy in the microscopic range.

Previously obtained results using the OPLS potential[7–9] are mainly subject to criticism because of the missing validity of the potential model in the microscopic range. This was recognized and in Ref. 7 the need for a better description of the intermolecular interaction is explicitly mentioned.

Structure calculations using the OPLS potential were performed from dimer to hexamer[8] and the main features agree with our results presented in Sec. III, i.e. the lowest energy dimer configuration is a chain structure, while from trimer to hexamer ring structures are found. For the energetically second lowest hexamer in both cases a ring configuration with C_2 symmetry is determined with a large energy gap to the other minimum energy configurations. In detail, however, there are distinct differences, especially for the lowest energy trimer and tetramer configurations. With the OPLS potential planar structures are found with C_{3h} and C_{4h} symmetry, respectively. Measurements of the OH stretch mode of size-selected trimers[16,18] and SCF calculations for methanol clusters[21,22] revealed, however, that this result is not correct. Instead an unsymmetrical ring structure is found for the trimer and a ring with S_4 symmetry for the tetramer which is in agreement with our results given in Sec. III.

Frequency shifts for the CO stretch and OH stretch mode from dimer to hexamer were calculated in various approximations using the OPLS potential.[7–9] Qualitative agreement with experimental results for the CO stretch mode was found and led to a misinterpretation of the trimer and tetramer spectrum. For the dimer OH stretch acceptor mode all calculations yield deviations from the experimental result of 100 cm^{-1} and more. This may partly be attributed to the deliberate overestimation of the static dipole moment in the OPLS model by about 25%.[20] Recently measured frequency shifts of the OH stretch mode of the trimer reveal[18] that the lowest energy configuration is, indeed, not planar and that calculations with better potential models are necessary.

SCF calculations for methanol clusters from dimer to hexamer are also available.[21,22] All symmetry features obtained for the lowest energy configurations are confirmed by the results obtained for the systematic potential in Sec. VI. Frequency shifts were calculated for the lowest energy configurations in the harmonic approximation and are given for the CO stretch mode by $-13\ \mathrm{cm}^{-1}$ and $12\ \mathrm{cm}^{-1}$ for the dimer, $-2\ \mathrm{cm}^{-1}$, $1\ \mathrm{cm}^{-1}$, and $9\ \mathrm{cm}^{-1}$ for the trimer, $-3\ \mathrm{cm}^{-1}$ and $1\ \mathrm{cm}^{-1}$ for the tetramer, $-3\ \mathrm{cm}^{-1}$, $-2\ \mathrm{cm}^{-1}$, $3\ \mathrm{cm}^{-1}$, $5\ \mathrm{cm}^{-1}$, and $11\ \mathrm{cm}^{-1}$ for the pentamer, and $-3\ \mathrm{cm}^{-1}$ and $4\ \mathrm{cm}^{-1}$ for the hexamer.[21] Note that the result for the dimer is quite close to the harmonic result obtained with the systematic potential at $-12\ \mathrm{cm}^{-1}$ and $16\ \mathrm{cm}^{-1}$. For a correction of the overall position of the two lines an anharmonic treatment is necessary which is, however, very expensive, since cubic and quartic force constants have to be calculated. For larger clusters the agreement with the experimental results is only qualitative. In particular no final conclusions can be drawn for the symmetry properties of the lowest energy trimer and tetramer configurations. Here an improvement could be achieved using the systematic potential, where a very nice agreement with the experimental data is found up to the tetramer.

The SCF harmonic frequencies for the OH stretch mode are given by $-3\ \mathrm{cm}^{-1}$ and $-78\ \mathrm{cm}^{-1}$ for the dimer, $-116\ \mathrm{cm}^{-1}$, $-120\ \mathrm{cm}^{-1}$, and $-150\ \mathrm{cm}^{-1}$ for the trimer, $-177\ \mathrm{cm}^{-1}$ and $-199\ \mathrm{cm}^{-1}$ for the tetramer, and $-203\ \mathrm{cm}^{-1}$ and $-250\ \mathrm{cm}^{-1}$ for the hexamer. Certainly an anharmonic treatment for the OH stretch mode is more important than it is for the CO stretch mode. Therefore it is no surprise that the SCF results for the trimer are in rather bad agreement with the experimental results. The necessity of the anharmonic treatment cannot be overemphasized.

In conclusion we note that a comparison to experimental results of size-selected methanol clusters for the CO stretch mode for heptamer and octamer and for the OH stretch mode from tetramer to nonamer will become available in a subsequent paper.[19] The cluster approach is a simple tool for calculating frequency shifts in quite complicated systems and yields reliable results providing that accurate intra- and intermolecular interaction potentials are used.

ACKNOWLEDGMENTS

This work is supported by the Deutsche Forschungsgemeinschaft in the Schwerpunktprogramm ''Molekulare Cluster.''

[1] D. J. Nesbitt, Chem. Rev. **88**, 843 (1988).
[2] J. R. Heath, R. A. Sheekes, A. L. Crosky, and R. J. Saykally, Science **249**, 855 (1990).
[3] T. E. Gough, R. E. Miller, and G. Scoles, J. Chem. Phys. **69**, 1588 (1978).
[4] R. E. Miller, Science **240**, 447 (1988).
[5] U. Buck and H. Meyer, J. Chem. Phys. **84**, 4854 (1986).
[6] U. Buck, Adv. Atom. Mol. Opt. Phys. **35**, 121 (1995).
[7] U. Buck and J. G. Siebers, Z. Phys. D **xx**, xxx (1997).
[8] U. Buck and B. Schmidt, J. Chem. Phys. **98**, 9410 (1993).
[9] T. A. Beu, Z. Phys. D **31**, 95 (1994).
[10] F. Huisken and M. Stemmler, Chem. Phys. **132**, 351 (1989).
[11] B. Heijmen, A. Bizarri, S. Stolte, and J. Reuss, Chem. Phys. **132**, 331 (1989).
[12] T. A. Beu and K. Takeuchi, J. Chem. Phys. **103**, 6394 (1995).
[13] T. A. Beu, U. Buck, J. G. Siebers, and R. J. Wheatley, J. Chem. Phys. **106**, 6795 (1997).
[14] T. A. Beu, U. Buck, I. Ettischer, M. Hobein, J. G. Siebers, and R. J. Wheatley, J. Chem. Phys. **106**, 6806 (1997).
[15] U. Buck, X. J. Gu, Ch. Lauenstein, and A. Randolph, J. Chem. Phys. **92**, 6017 (1990).
[16] F. Huisken and M. Stemmler, Chem. Phys. Lett. **144**, 391 (1987).
[17] F. Huisken, A. Kulcke, C. Laush, and J. M. Lisy, J. Chem. Phys. **95**, 3924 (1991).
[18] F. Huisken, M. Kaloudis, M. Koch, and O. Werhahn, J. Chem. Phys. **105**, 8965 (1996).
[19] U. Buck and I. Ettischer, J. Chem. Phys. **108**, 33 (1998), following paper.
[20] W. L. Jorgensen, J. Phys. Chem. **90**, 1276 (1986).
[21] J. Sauer and A. Bleiber, Polish J. Chem. (submitted).
[22] O. Mó, M. Yáñez, and J. Elguero, J. Mol. Struct.: THEOCHEM **314**, 73 (1994).
[23] F. Bernardi, H. B. Schlegel, and S. Wolfe, J. Chem. Phys. **67**, 4181 (1977).
[24] A. J. Stone, Chem. Phys. Lett. **83**, 233 (1981).
[25] R. D. Amos, I. L. Alberts, J. S. Andrews, S. M. Colwell, N. C. Handy, D. Jayatilaka, P. J. Knowles, R. Kobayashi, N. Koga, K. E. Laidig, P. E. Maslen, C. W. Murray, J. E. Rice, J. Sanz, E. D. Simandiras, A. J. Stone, and M.-D. Su, CADPAC5, Issue 5, University of Cambridge, 1992.
[26] S. L. Price, A. J. Stone, and M. Alderton, Mol. Phys. **52**, 987 (1984).
[27] Dipole quoted as 0.665 atomic units, and polarizability as 22 atomic units, by C. Huiszoon, Mol. Phys. **58**, 865 (1986).
[28] R. J. Wheatley and J. B. O. Mitchell, J. Comput. Chem. **15**, 1187 (1994).
[29] R. J. Wheatley and S. L. Price, Mol. Phys. **69**, 507 (1990).
[30] Quoted from the work of B. L. Jhanwar and W. J. Meath, by M. A. Spackman, J. Chem. Phys. **94**, 1295 (1991).
[31] G. D. Zeiss and W. J. Meath, Mol. Phys. **33**, 1155 (1977).
[32] M. Massucci, A. P. du'Gay, A. M. Diaz-Laviada, and Ch. J. Wormald, J. Chem. Soc. Faraday Trans. **88**, 427 (1992).
[33] D. J. Evans and R. O. Watts, Mol. Phys. **28**, 1233 (1974).
[34] A. H. Stroud, *Approximate Calculation of Multiple Integrals* (Prentice–Hall, Englewood Cliffs, NJ, 1971), p. 87.
[35] B. H. Torrie and S. X. Weng, Mol. Phys. **67**, 575 (1989).
[36] J. K. G. Watson, Mol. Phys. **15**, 479 (1968).
[37] I. M. Mills, in *Molecular Spectroscopy: Modern Research*, edited by K. Narahari Rao and C. W. Mathews (Academic Press, New York, 1972).
[38] U. Buck and I. Ettischer, J. Chem. Phys. **100**, 6974 (1994).